

Neutron Transfer Reactions for Deformed Nuclei Using Sturmian Basis

V. G. Gueorguiev¹, P. D. Kunz², J. E. Escher¹, F. S. Dietrich¹

¹Lawrence Livermore National Laboratory, Livermore, California, USA

²Department of Physics and Astrophysics, University of Colorado, Boulder, Colorado, USA

(Dated: August 10, 2021, UCRL-JRNL-231626)

We study the spin-parity distribution $P(J^\pi, E)$ of ^{156}Gd excited states above the neutron separation energy that are expected to be populated via the neutron pickup reaction $^{157}\text{Gd}(^3\text{He}, ^4\text{He})^{156}\text{Gd}$. In general, modeling of the spin-parity distribution is important for the applicability of the surrogate reaction technique as a method of deducing reaction cross sections. We model excited states in ^{156}Gd as rotational states built on intrinsic states consisting of a hole in the core where the hole represents neutron removal from a deformed single particle state. The reaction cross section to each excited state is calculated using standard reaction code that uses spherical reaction form-factor input. The spectroscopic factor associated with each form-factor is the expansion coefficient of the deformed neutron state in a spherical Sturmian basis consisting of the spherical reaction form-factors.

PACS numbers: 21.10.Jx, 24.50.+g, 24.10.Eq, 25.55.Ci

I. INTRODUCTION AND MOTIVATION

Most light nuclei up to C and O are produced via nuclear reactions within the stars. Heavier nuclei near the valley of stability are produced via slow neutron capture process (s process). To account for the observed abundance of the elements, however, one needs to also consider other processes such as proton capture process (p process) and rapid neutron capture process (r process). The r process is essential in the production of the heaviest neutron rich elements since this process generates nuclei far from the valley of stability that decay back towards the valley. Successively heavier neutron rich nuclei are produced through violent processes such as supernova explosions. Such nuclei usually decay quickly. As a consequence, the understanding of the r-process contribution to the observed abundance of the elements requires knowledge of the neutron induced reactions on unstable nuclei. Unfortunately, measuring these cross sections in a laboratory environment is a very difficult, if not impossible, task because of the technical and practical problems associated with the use of an unstable nuclei.

There have been various proposals for circumventing the problems associated with the use of unstable nuclei and yet to gain information about the desired nuclear reaction. One such approach is the Surrogate Method shown schematically in Fig. 1.

In this paper we study the reaction $^3\text{He} + ^{157}\text{Gd} \rightarrow ^4\text{He} + ^{156}\text{Gd}^*$ and model the formation probability of various excited states of the ^{156}Gd system within a direct reaction framework. This reaction is a testing ground of the surrogate method for the neutron capture reaction $^{155}\text{Gd} + n \rightarrow ^{156}\text{Gd}^*$. Thus, one has to study the surrogate reaction for excitation energies E_{ex} of ^{156}Gd that correspond to few MeV neutron absorption in ^{155}Gd ($0 < E_n < 2$); by energy balance one has: $E_{ex} = M_{^{155}\text{Gd}} + M_n + E_n - M_{^{156}\text{Gd}} = S_n + E_n$ where M is the corresponding rest mass and $S_n = 8.536$ MeV is the neutron separation energy for ^{156}Gd [1]. Therefore, we

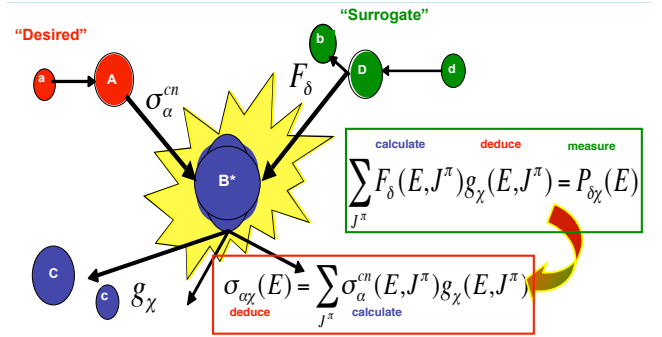


FIG. 1: Reaction cross section for the desired reaction $a+A \rightarrow B^* \rightarrow C+c$ might involve an unstable target A. Alternatively, the cross section may be deduced using theoretical modeling and experimental data from a surrogate reaction $d+D \rightarrow b+B^* \rightarrow C+c$ on a stable target D. Both reactions proceed via the formation of the same intermediate compound system B^* .

shall focus on excited states in ^{156}Gd such that:

$$E_{ex}^{^{156}\text{Gd}} > 8.5 \text{ MeV}. \quad (1)$$

II. MATHEMATICAL FRAMEWORK

Atomic nuclei exhibit a multitude of spectral phenomena. Among the simplest and relatively well understood properties are the rotational and vibrational spectra as well as the general single-particle shell structure that explains the observed magic numbers [2, 3]. The traditional modeling of deformed even-even nuclei considers the rotational states of nuclei as a collective phenomenon whose states are simple rotational functions [3]. An extra particle is then assumed to occupy a valence single particle state within a deformed mean-field potential. This allows one to treat the odd-even deformed nuclei within the rotor plus single particle model. Within this framework one can calculate cross sections for particle transfer as transi-

tion amplitudes between collective rotational states and a particle plus rotor states.

A. States of axially deformed nuclei

1. Bohr-Mottelson rotor model for deformed nuclei

Within the rotor model an intrinsic state of a deformed system, with axial symmetry, gives rise to a rotational band with energies and wave functions of the form [3]:

$$\begin{aligned} J &= K, K + (1 + \delta_{K,0}), K + 2(1 + \delta_{K,0}), \dots \\ E(J) &= E_K + \frac{\hbar^2}{2\mathcal{I}}(J(J+1) - K(K+1)), \quad (2) \\ \Psi_{KJM} &= \frac{1}{4\pi} \sqrt{\frac{J(J+1)}{(1 + \delta_{K,0})}} \times \\ &\times [D_{MK}^J(\omega)\Phi_K + (-1)^{K+J}D_{M-K}^J(\omega)\Phi_{\bar{K}}]. \end{aligned}$$

Here \mathcal{I} is the moment of inertia of the system, which for simplicity is assumed to be independent of K , ω stands for the angles θ and ϕ , D_{MK}^J are the rotational matrices, $\Phi_{\bar{K}}$ is the reflection of the intrinsic state Φ_K with respect to the symmetry axis, and K is the angular momentum projection onto the symmetry axis.

2. Rotor plus particle/hole system

In the zero order approximation where, we neglect possible particle-core couplings such as Coriolis coupling, the combined system of a particle/hole plus a core has an intrinsic state Φ_Ω that can be viewed as a direct product of the intrinsic state of the core Φ_K^{cor} and the single particle/hole state ψ_ν :

$$\Phi_\Omega = \psi_\nu \Phi_K^{cor}, \quad E_\Omega = E_K + \epsilon_\nu. \quad (3)$$

where $\Omega = K + \nu$ due to axial symmetry. Therefore, for the particle plus core system we have:

$$\begin{aligned} J &= \Omega, \Omega + (1 + \delta_{\Omega,0}), \Omega + 2(1 + \delta_{\Omega,0}), \dots \\ E(J) &= E_\Omega + \frac{\hbar^2}{2\mathcal{I}}(J(J+1) - \Omega(\Omega+1)), \quad (4) \\ \Psi_{\Omega JM} &= \frac{1}{4\pi} \sqrt{\frac{2J+1}{(1 + \delta_{\Omega,0})}} \times \\ &\times [D_{M\Omega}^J(\omega)\Phi_K\psi_\nu + (-1)^{\Omega+J}D_{M-\Omega}^J(\omega)\Phi_{\bar{K}}\psi_{\bar{\nu}}]. \end{aligned}$$

As long as the final states that we are interested in are assumed to be built out of the same initial intrinsic core state, we can make perturbation adjustments, presumably small, to the single particle energies to incorporate BCS pairing and Coriolis coupling effects.

B. Single particle states in axially deformed nuclei

Since the nucleon density in nuclei is constant, except near the nuclear surface, one expects that the general form of the mean-field potential, which defines the single particle states, is of Woods-Saxon type [4]:

$$V(r) = \frac{V_0}{1 + \exp\left(\frac{r-R}{a}\right)} \quad (5)$$

For spherical nuclei R is constant and represents the position of the nuclear surface while a is related to the diffuseness of the potential near the surface. For deformed nuclei, however, R depends on the surface point of interest and is often parametrized using spherical harmonics:

$$R(\theta, \phi) = R_0 \left(1 + \sum_{\lambda\mu} a^{\lambda\mu} Y_{\lambda\mu}(\theta, \phi) \right) \quad (6)$$

For axially deformed nuclei R does not depend on ϕ due to the axial symmetry. The $\lambda = 1$ is absent due to center of mass considerations and odd λ terms are usually absent due to parity considerations; for axially deformed nuclei one usually assumes quadrupole and hexapole deformation only:

$$R(\theta, \phi) = R_0 (1 + \beta_2 Y_{20}(\theta, \phi) + \beta_4 Y_{40}(\theta, \phi)) \quad (7)$$

1. Single particle states at small deformation

For small values of the deformation parameters $\beta \lesssim 0.3$ in (7) one can expand the Woods-Saxon potential (5) in Taylor series. The simplest approach is to consider only the first order terms in the expansion [5].

$$V(r, R) \simeq V(r, R_0) - V'(r, R_0) \frac{R_0}{a} (\beta_2 Y_{20}(\theta, \phi) + \dots) \quad (8)$$

While in many cases this seems to be sufficient, some particular single particle states are sensitive to small deformation values of beta $\beta_2 \lesssim 0.1$.

2. Single particle levels at strong deformation

If β is sufficiently small, so that the Taylor expansion converges, one can re-express $V(r, R)$ in multiple expansion in terms of spherical harmonics [6]. An alternative way is to solve numerically the Schrödinger equation for the deformed Woods-Saxon potential [7]. When comparing the single particle energies calculated numerically to the one calculated using only first order Taylor expansion approximation, one finds that for rare-earth nuclei (nuclei near Gd) the “Nilsson diagrams” agree for $\beta_2 \lesssim 0.1$ but start to deviate at larger deformations; in particular, there is a substantial deviation for $m_j = j$ states.

To understand the impact of the deformation and what should be considered as a small deformation, calculations

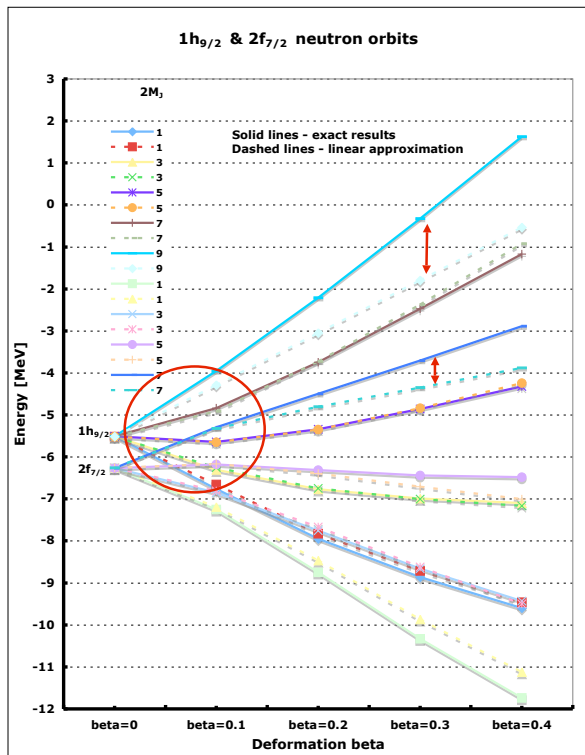


FIG. 2: ^{157}Gd deformed single particle energies as function of the deformation β for $V_0=-44.6883$ MeV, $r_0=1.27$ fm, $a_0=0.67$ fm, $V_{is}=15.9945$ MeV. The circle indicates the region of agreement between the linear treatment and the exact numerical treatment. The arrows at $\beta = 0.3$ indicate the most substantial deviation, between the linear treatment and the exact numerical treatment, observed for the $j = m = 9/2$ and $j = m = 7/2$ states.

were performed using several codes [5, 7, 8, 9, 10, 11, 12]. First we made sure that in the case of zero deformation the low energy spectrum agrees well within few keV. In most cases an initial disagreement was fixed by improving the treatment of the reduced mass of the particle-core system. We also found that the choice of the spin-orbit interaction could result in a factor of about 2 or 4 depending on the convention used. Usually obtaining the $p_{1/2}$ and $p_{3/2}$ splitting is the main indication that the factor affecting the strength of the spin-orbit term is properly accounted for. The energy of the $s_{1/2}$ state was used for understanding the convention for the strength of the central potential. When the energies of the $s_{1/2}$, $p_{1/2}$, and $p_{3/2}$ states are reproduced, by each of the codes and the reduced mass is properly accounted for, the rest of the bound spectrum is usually well reproduced within few keV. For small non-zero deformation we used fewer

codes [5, 7, 9, 10], while for large deformation we relied only on [7].

Fig 2 shows the dependence of the single particle energies of the $nl_j = 1h_{9/2}$ and $2f_{7/2}$ orbitals. Calculations using a code that treats the interaction as linear in the deformation (8) are compared to an exact numerical treatment of the interaction [5, 7]. Fig 2 illustrates that one has to treat deformation with caution.

In Table I are shown the neutron bound states in ^{157}Gd calculated using deformed Woods-Saxon potential [13]. Since we have used WSBETA code [7], which uses an exact numerical method instead of a linear approximation, we have set $\beta_4 = 0$ which gives the binding energy of the 47th neutron single particle state close to the experimental neutron separation energy ($S_n = 6.3598$ MeV [14]) in ^{157}Gd $\epsilon_{47} = -6.361$ MeV.

ν	ϵ_ν [MeV]	J^π	ν	ϵ_ν [MeV]	J^π	ν	ϵ_ν [MeV]	J^π
1	-39.971	$\frac{1}{2}^+$	23	-16.900	$\frac{1}{2}^-$	45	-7.054	$\frac{11}{2}^+$
2	-36.357	$\frac{1}{2}^-$	24	-16.814	$\frac{1}{2}^+$	46	-6.820	$\frac{3}{2}^+$
3	-34.665	$\frac{3}{2}^-$	25	-16.809	$\frac{7}{2}^+$	47	-6.361	$\frac{3}{2}^-$
4	-34.036	$\frac{1}{2}^-$	26	-14.870	$\frac{1}{2}^+$	48	-5.980	$\frac{5}{2}^+$
5	-31.655	$\frac{1}{2}^+$	27	-14.867	$\frac{3}{2}^+$	49	-5.563	$\frac{5}{2}^-$
6	-30.453	$\frac{3}{2}^+$	28	-14.661	$\frac{9}{2}^+$	50	-5.000	$\frac{1}{2}^-$
7	-29.441	$\frac{1}{2}^+$	29	-13.953	$\frac{1}{2}^-$	51	-4.795	$\frac{7}{2}^+$
8	-28.570	$\frac{3}{2}^+$	30	-13.408	$\frac{3}{2}^-$	52	-4.290	$\frac{5}{2}^-$
9	-26.745	$\frac{3}{2}^+$	31	-12.608	$\frac{3}{2}^+$	53	-3.284	$\frac{9}{2}^+$
10	-26.230	$\frac{1}{2}^-$	32	-12.424	$\frac{5}{2}^-$	54	-2.846	$\frac{7}{2}^-$
11	-26.045	$\frac{1}{2}^+$	33	-12.286	$\frac{5}{2}^+$	55	-2.706	$\frac{1}{2}^+$
12	-25.345	$\frac{3}{2}^-$	34	-11.239	$\frac{5}{2}^+$	56	-2.655	$\frac{1}{2}^-$
13	-23.895	$\frac{3}{2}^-$	35	-11.051	$\frac{7}{2}^-$	57	-2.072	$\frac{3}{2}^-$
14	-23.609	$\frac{1}{2}^-$	36	-9.986	$\frac{5}{2}^+$	58	-1.951	$\frac{7}{2}^-$
15	-21.863	$\frac{7}{2}^-$	37	-9.518	$\frac{1}{2}^-$	59	-1.427	$\frac{11}{2}^+$
16	-21.349	$\frac{3}{2}^-$	38	-9.290	$\frac{9}{2}^-$	60	-1.296	$\frac{3}{2}^+$
17	-20.911	$\frac{1}{2}^-$	39	-8.994	$\frac{7}{2}^+$	61	-0.820	$\frac{1}{2}^+$
18	-20.294	$\frac{1}{2}^+$	40	-8.137	$\frac{1}{2}^-$	62	-0.716	$\frac{3}{2}^-$
19	-19.616	$\frac{3}{2}^+$	41	-8.053	$\frac{1}{2}^+$	63	-0.390	$\frac{1}{2}^-$
20	-18.437	$\frac{5}{2}^+$	42	-7.811	$\frac{3}{2}^-$	64	-0.131	$\frac{1}{2}^-$
21	-18.321	$\frac{5}{2}^-$	43	-7.591	$\frac{3}{2}^+$	65	0.015	$\frac{3}{2}^-$
22	-18.009	$\frac{3}{2}^-$	44	-7.276	$\frac{1}{2}^+$	66	0.400	$\frac{5}{2}^+$

TABLE I: Neutron bound states in ^{157}Gd calculated with the WSBETA code [7] using Woods-Saxon parameters from Ref. [13] but $\beta_4 = 0$ so that the 47th neutron state ($\epsilon_{47} = -6.361$) is near the experimental neutron separation energy $S_n = 6.3598$ MeV [14], $V_0=-45.1776$ MeV, $r_0=1.25$ fm, $a_0=0.65$ fm, $V_{is}=19.2015$ MeV, $\beta_2 = 0.29$ and $\beta_4 = 0$. The Fermi level and the level that results in excitation near the neutron separation energy in ^{156}Gd ($S_n = 8.536$ MeV) are in boldface and marked by two horizontal lines.

C. Adjustments to the single particle energies

In the Distorted Wave Born Approximation (DWBA) the single particle wave function of the transferred particle is of essence along with the probability amplitude of the particle to be in that state. Ideally one would calculate the many body eigenstates of the initial and final system within a chosen single particle basis and then would deduce the probability amplitude - the spectroscopic factor for the single particle to be in any of the single particle states. Such approach has the advantage that a many body Hamiltonian that describes the initial and the final systems is used to deduce the single particle wave function of the transferred particle. However, finding the many body Hamiltonian that works equally well across the nuclear chart has proven elusive.

The absence of clearly successful and unique many body Hamiltonian and method for solving the many body problem justifies the use of simpler models for deducing the single particle wave function of the transferred particle such as the particle plus core model described in section II A. There are some issues with such models. For example, the total anti-symmetrization, pairing interaction, and particle-core interaction effects are points to be addressed. The effect of the anti-symmetrization is usually taken into account within the DWBA calculation by using the appropriate combinatorial factors [15]. The particle-core interaction is usually dominated by a Coriolis coupling and the pairing effects within the core are accounted for through the BCS pairing model. Other interaction such as coupling to the quadrupole vibrations of the core will not be considered here [16].

1. BCS pairing

The pairing interaction is a many body phenomenon which is effectively an interaction between pairs of time conjugated particles. Exact solutions of the pairing and its variations are well known [17, 18, 19]. However, an approximation know as BCS paring is very convenient [20]. Since the pairing interaction is effectively pair creation and annihilation process its main effect is on the occupation of the single particle states near the Fermi energy that represents the location of the last occupied state and next unoccupied state. This means that the occupation number n_ν of states that are sufficiently far from the Fermi energy μ are practically not affected by the paring.

$$n_\nu = 1 - \frac{\epsilon_\nu - \mu}{\sqrt{(\epsilon_\nu - \mu)^2 + \Delta^2}} \quad (9)$$

Fig. 3 shows the occupation number n_ν by applying the BCS equations to the set of single particle energies shown in Table I. From the graph one can see that the occupation of the particle levels with energies $\epsilon_\nu < -9$ MeV are practicly unaffected by the pairing interaction.

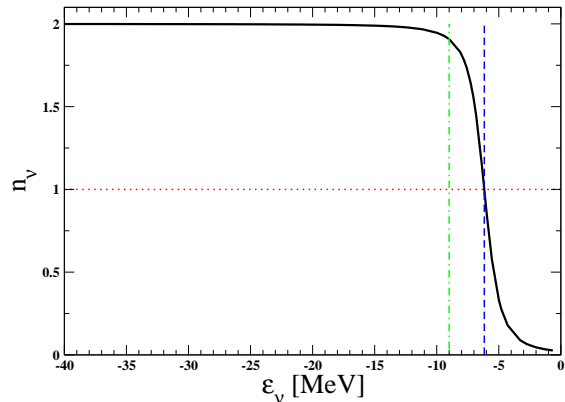


FIG. 3: Occupation number n_ν for single particle bound states ϵ_ν in the ^{157}Gd system. Single particle energies ϵ_ν are calculated for deformed Woods-Saxon potential with parameters: $V_0 = -45.1776$ MeV, $r_0 = 1.25$ fm, $a_0 = 0.65$ fm, $V_{1s} = 19.2015$ MeV, deformation $\beta_2 = 0.29$ and the following BCS parameters: Fermi energy $\mu = -6.169$ MeV, pairing gap $\Delta = 1.307$ MeV, and pairing strength $g = 0.15$ MeV.

Notice that according to (1) one has to pull out neutrons that are at least 8 MeV below the Fermi level:

$$\epsilon_\nu < -14.9 \text{ MeV}. \quad (10)$$

For this BCS calculation, we used all neutron bound states in ^{157}Gd except the 47^{th} state which is assumed to be Pauli blocked to the pairing interaction due to the odd nucleon. The Fermi energy μ was chosen to be between the last occupied state and the first unoccupied state in the system $\mu = (\epsilon_{47} + \epsilon_{48})/2$. The values of the pairing gap Δ and the pairing strength g were determined from the BCS equations.

2. Particle core coupling

It is well know that the Coriolis coupling is an important interaction [21, 22, 23, 24].

$$H_C = -\frac{\hbar^2}{2I}(I_+j_- + I_-j_+) \quad (11)$$

The proper consideration results in Coriolis band mixing and technical complications similar to the shell model wave function type approach. It is known that the first order perturbation to the energy is non-zero for $\Omega = \frac{1}{2}$ bands only and higher order terms are needed to obtain the energy shifts in $\Omega > \frac{1}{2}$ bands [21, 22].

For this study, however, we consider only one intrinsic state of the core (the ground state of the target) coupled to various neutron holes in the core. This, therefore, eliminates any Coriolis band mixing from our model.

There is, however, an important particle/hole core coupling that we estimate by using first order perturbation approximation. This gives us the energy splitting between the states $\Omega = |K - \nu|$ and $\Omega = K + \nu$. It is clear that according to the simple non-interaction particle plus rotor model (3), we have two degenerate states $\Omega = |K - \nu|$ and $\Omega = K + \nu$. To estimate the splitting of these two states, due to rotation, we look at the expectation value of the rotational energy of the particle plus core system in the intrinsic frame (3):

$$\begin{aligned} & \langle \Omega = K \pm \nu | (\vec{J}_{cor} + \vec{j}_p)^2 | \Omega = K \pm \nu \rangle = \\ & = \langle K | \vec{J}_{cor}^2 | K \rangle + \langle \nu | \vec{j}_p^2 | \nu \rangle + \\ & \quad + 2 \langle \Omega = K \pm \nu | \vec{J}_{cor} \cdot \vec{j}_p | \Omega = K \pm \nu \rangle = \\ & = \langle K | \vec{J}_{cor}^2 | K \rangle + \langle \nu | \vec{j}_p^2 | \nu \rangle \pm 2K\nu. \end{aligned}$$

Since the first two terms are the same and represent the rotational energy of the core and the particle, one expects the energy splitting to be:

$$\Delta E(\Omega_{\pm} = |K \pm \nu|) = \pm c \frac{\hbar^2}{2\mathcal{I}} K\nu. \quad (12)$$

Here c is a coefficient that relates the moment of inertia around the symmetry axis z to the moment of inertia around x and y axes. One could estimate its value from the mathematical expressions for the moment of inertia of a rigid ellipsoid as given in the Appendix section V A. Here, however, we prefer phenomenological adjustment that reproduces the experimentally observed splitting between $\Omega = 0$ and $\Omega = 3$ bands in ^{156}Gd by using the experimental moment of inertia \mathcal{I} needed to reproduce the $\Omega = 0$ ground state band.

D. Reaction cross sections for deformed nuclei

1. DWBA direct reactions within the Optical Model Potential (OMP) theory

The Distorted Wave Born Approximation (DWBA) considers the initial (final) state of the system to be a product of initial $|A, a \rangle$ (final $|B, b \rangle$) intrinsic states of the target, projectile, and distorted wave function χ^{\pm} that depends on the relative coordinates between the target and the projectile [11, 12, 15]. The reaction cross section is then calculated using an Optical Model Potential (OMP) for χ^{\pm} and the appropriate nuclear interaction V relating the initial state $|A, a \rangle$ with the final state final $|B, b \rangle$. The transition amplitude then depends on the corresponding interaction matrix $\langle Bb | V | Aa \rangle$. For one-nucleon transfer reactions this matrix element depends on the initial and final state of the transferred nucleon, the particular interaction that connects these states, and the overlap of the other nucleons. For a neutron pickup reaction, it reduces to: the neutron wave function ψ inside the target, the strength D_0 of a zero range δ force interaction with the projectile, and a spectroscopic factor

$S^{1/2}$ showing how much the target A looks like a remnant B plus a nucleon in the state ψ ($\langle A | \psi^\dagger B \rangle$).

2. Separation energy matching method for proper tail of the single spherical states

For transfer reactions that result in low energy excited states the correct asymptotic tail of the wave function, which is related to the neutron separation energy, is very important in neutron pickup since one expects that the last (outer most) nucleon is being transferred. Using wave functions that have the desired binding energy by adjusting the depth of the Woods-Saxon binding potential is one of the simplest and usually very successful approximations for calculating the reaction cross section. In this approach one keeps the geometric factors of the binding potential, such as r_0 and a_0 of the potential, fixed from systematics but changes the depth of the potential until a bound state ψ with the desired binding energy is found. The approach has even been extended to the point where the variable parameter is the strength of a surface derivative potential.

3. Sturmian method for form-factors

Problems with the separation energy matching using only one spherical wave function has been a motivation for more accurate description of the relevant form factor by inclusion of more than one basis state. The spherical harmonic oscillator (SHO) is a traditional basis to expand a wave function. However, the tail in a finite SHO basis expansion is always wrong. An interesting alternative basis to expand a deformed bound state is to use the set of bound states of the spherical part of the interaction [13]. However, this expansion does not guarantee correct tail either. An expansion would provide the correct tail if one of the basis states is a bound state with the same energy as the state that is being expanded and all the other non zero components correspond to basis states with a deeper binding energy.

In a Sturmian basis all the basis states have the same tail as the original state that is being expanded in this basis. In order to maintain correct asymptotic tail one is now facing a problem where one has to find different wave functions and potential strengths that result in the same energy and thus the same wave function tail. The Sturmian basis method has been utilized before [25]. The method in [25] relies essentially on expressing the deformed potential as linear in β_2 which may not be sufficient in the case of strong deformation. Unfortunately, this approach relies on the linear form of the potential with respect to the deformation parameters.

Another, more successful and physically more appealing approach is to consider coupled channel (CC) calculations [10]. Unfortunately, this code in its current version has only β_2 deformation. In one of the next section we

will discuss briefly our comparison to this code and possible further developments.

To illustrate the role of various parameters involved, we now look at the incoherent DWBA reaction cross section for a particle transfer from a deformed single particle state ψ_ν that can be expressed in terms of transfer cross sections on spherical single particle states ϕ_{nlj} [15, 25]:

$$d\sigma(J_i K_i \rightarrow J_f K_f; \nu) = \sum_{lj} \sum_n (a_\nu v_\nu c_\nu^{nlj})^2 d\sigma_{nlj}^{DW} \quad (13)$$

Here σ_{nlj}^{DW} are the DWBA cross section from a spherical state ϕ_{nlj} , c_ν^{nlj} are the expansion coefficients of the state ψ_ν in spherical basis states ϕ_{nlj} , v_ν represents BCS occupation number ($v_\nu^2 = n_\nu/2$) of the state ν , and a_ν is the Coriolis band mixing amplitude. The spectroscopic factor S_{lj} is often used as shorthand notation for the term raised to second power. In our calculations, we actually consider the generally more appropriate coherent cross section by using super-position of basis states ϕ_{nlj} with amplitudes $a_\nu v_\nu c_\nu^{nlj}$.

III. NEUTRON TRANSFER REACTION RESULTS

In this section we present the results of our calculations on the neutron transfer reaction $^{157}\text{Gd}(^3\text{He}, ^4\text{He})^{156}\text{Gd}$. We first discuss the OMP for the in-going and out-going channels, then we show the excited states in ^{156}Gd according to the particle plus rotor model which in this case is actually a hole in the core model. Next we briefly discuss the model space convergence in the determination of the c_ν^{nlj} amplitudes. After that the absolute cross sections and their convergence are discussed along with a smeared $\sigma(E)$ cross section profile near the neutron separation energy. Finally, we turn to a discussion of the probability distributions $P(J^\pi, E)$.

Our transfer cross sections related to the reaction $^{157}\text{Gd}(^3\text{He}, ^4\text{He})^{156}\text{Gd}$ are for one nucleon removal from a deformed single particle state ψ_{ϵ_ν} from the ^{157}Gd system viewed as a core in a $K = 3/2^-$ state. Presumably, the final states of the ^{156}Gd system are rotational states built on the intrinsic state Ω just like in the particle plus core model (3). However, instead particles we work with holes in the core $|A = 156, \Omega \rangle = \psi_\nu^\dagger |A = 157, K = 3/2^- \rangle$.

A. Elastic cross sections and the optical model parameters

Usually, calculations with distorted waves within the DWBA use an Optical Model Potential (OMP):

$$U = Vf(x_0) + iWf(x_w) - V_{so} \frac{1}{r} \frac{df(x_{so})}{dr} \vec{l} \cdot \vec{s}$$

$$f(r) = \frac{1}{1 + \exp((r - R)/a)}, \quad R = r_0 A^{1/3}$$

Table II shows the OMP parameters used in our calculation. These parameters are taken from the Reference Input Parameter Library (RIPL-2) [26]. The Rutherford normalized elastic cross sections for the in-going and out-going channels are shown in Fig. 4. Notice that the absence of interference pattern for the ^3He cross section is due to its relatively low energy.

Reaction	r_c	V	r_0	a_0	W	r_w	a_w	V_{so}	r_{so}	a_{so}
$^3\text{He} + ^{157}\text{Gd}$	1.3	154	1.2	0.72	36	1.4	0.88	2.5	1.2	0.72
$^4\text{He} + ^{156}\text{Gd}$	1.2	159	1.2	0.8	14	1.6	0.7	0	1.2	0.8

TABLE II: OMP parameters, in fm and MeV units, for the in-going $^3\text{He} + ^{157}\text{Gd}$ [27] and the out-going $^4\text{He} + ^{156}\text{Gd}$ [28].

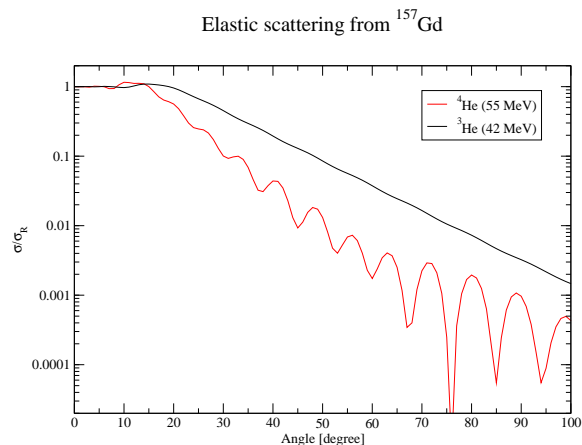


FIG. 4: Rutherford normalized elastic cross sections for the relevant He+Gd reaction. The smoothness of the ^3He cross section is due to the lower value of the associated energy.

B. Excited states in ^{156}Gd according to the hole in the core model

In calculating a transfer reaction to an excited state in ^{156}Gd , we first construct an intrinsic state in ^{156}Gd as a hole in the ^{157}Gd core then we consider rotational states built on that intrinsic state. We consider total of 12 members of the related $\Omega = |K \pm \nu|$ rotational bands to include all possible excitations with $J < 8$.

$$|^{156}\text{Gd}, \Omega = |K \pm \nu| \rangle = \psi_{\pm\nu}^\dagger |^{157}\text{Gd}, K = 3/2^- \rangle \quad (14)$$

$$E(J^\pi; \Omega = |K \pm \nu|) = \epsilon_0 - \epsilon_\nu + \frac{\hbar^2}{2\mathcal{I}} (J(J+1) + \delta_\pm)$$

Here ϵ_0 is used to set the ground state energy of ^{156}Gd to zero, and δ_\pm is the energy shift of the $\Omega = K + \nu$ state relative to the $\Omega = |K - \nu|$ state. Thus if we set $\delta_- = 0$ for $\Omega = |K - \nu|$ then $\delta_+ = 2cK\nu$ for $\Omega = K + \nu$ states.

We always keep Ω , ν , and K positive when we use them as quantum numbers of the states.

By fitting the first four excited states of the $\Omega = 0^+$ ground state band, the moment of inertia is fixed to be $\hbar^2/2\mathcal{I} = 13.59$ KeV for the rotational bands in ^{156}Gd . The $c = 17.741$ coefficient for the energy shift (12) of the related $\Omega = 3^+$ band was chosen to reproduced the excitation energy of the 3_1^+ state. The value of c is about 1.65 times the ratio of the moments of inertia $\mathcal{I}_{\parallel}/\mathcal{I}_{\perp}$ for rigid ellipsoid with $\beta = 0.29$. In Table III is shown comparison of the experimentally observed low energy states in ^{156}Gd [14] and excitation energies calculated considering a neutron hole coupled to a core.

J_n^π	E_{exp} [MeV]	E_{th} [MeV]	J_n^π	E_{exp} [MeV]	E_{th} [MeV]
0_{gs}^+	0	0.004	3_1^+	1.248	1.255
2_1^+	0.089	0.085	4_3^+	1.355	1.363
4_1^+	0.288	0.275	5_1^+	1.507	1.499
6_1^+	0.585	0.574	6_3^+	1.644	1.662
8_1^+	0.965	0.982	7_1^+	1.85	1.852

TABLE III: Comparison of the experimentally observed low energy states in ^{156}Gd [14] and excitation energies calculated considering a neutron hole $\nu = 3/2^-$ at $\epsilon_{47} = -6.361$ coupled to the core system ^{157}Gd with $K = 3/2^-$. The first three columns represent the $\Omega = 0^+$ ground state band; the next three columns represent the $\Omega = 3^+$ band. The theoretical ground state is not exactly zero because ϵ_{47} is not exactly equal the neutron separation energy S_n in ^{157}Gd .

In Fig. 5 are shown the parity (π), angular momentum (J), and energy (E) of the states that are considered in the calculations of the reaction cross sections $\sigma(J^\pi; E)$. The absence of positive parity states in the 10 MeV region is due to the five positive parity single particle states 24-28 with energy between -16.81 and -14.66 in Table I. These states will produce a parity asymmetry in the $P(J^\pi, E)$ distribution in the energy region of interest for the surrogate method.

C. Model space convergence

In order to compute the transfer cross section one needs the single particle wave function and the corresponding spectroscopic factor. We already discussed our main approximations to the spectroscopic factor: we neglect the Coriolis band mixing ($a_\nu = 1$), the pairing effects ($v_\nu = 1$), and consider single particle wave functions that are expressed in a Sturmian basis. The idea is to maintain the same exponential tail for each spherical basis state as the tail of the deformed state that we are interested in. We have to make expansion in a spherical basis in order to be able to use existing reaction codes.

Here we consider the Sturmian approach by using Sturmian spherical basis states. We calculate the spectra of a deformed Woods-Saxon potential using standard bound states technique code WSBETA [7]. Then for each state

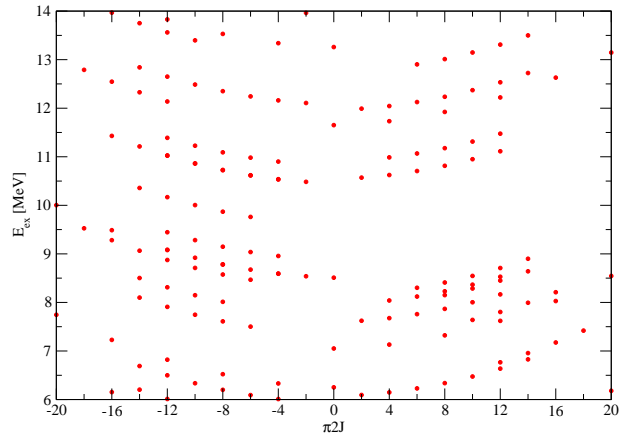


FIG. 5: Distribution of the calculated ^{156}Gd excited states. The sign of the x-axis encodes the parity of the states and the magnitude is equal to the twice of the angular momentum J .

ψ_ν with energy ϵ we find all the Sturmian spherical basis states (zero deformation) $\phi_{\epsilon nlj}$ with nlj labels as for a spherical harmonic oscillator up to the N_{max} oscillator shell. These basis states are constructed with the reaction code DWUCK4 [11]. For a fixed ϵ and nlj labels the code finds a scaling factor for the original spherical potential such that $\phi_{\epsilon nlj}$ is a bound state of this new potential. This scaling factor is then used to recompute the state $\phi_{\epsilon nlj}$ within the WSBETA code in the same basis where the deformed state ψ_ν has been computed. The expansion amplitudes c_ν^{nlj} are then calculated as described in the Appendix Section VB and then passed back to the reaction code to compute the cross section for pickup from the deformed state ψ_ν using the spherical basis states $\phi_{\epsilon nlj}$. Since the c_ν^{nlj} amplitudes have to be added coherently, we have used the coupled channel code CHUCK3 [12].

In order to test the reliability of our amplitudes and the corresponding radial wave functions, we have compared some of our c_ν^{lj} and $\phi_{\epsilon lj}$ against calculations with the Rost's code [10]. The agreement is good but not perfect; discrepancies can be attributed to differences in the implementation of the non-zero deformation.

In order to understand how well a state ψ_ν is expressed in the corresponding Sturmian basis one has to study the norm of ψ_ν in the Sturmian basis and how this norm converges with the size of the model space. From Fig. 6 one can clearly see the model space convergence.

The state norm converges even faster. Beyond $N_{max} = 10$ the smallest non unit norm is only 0.98. Unfortunately, there are some particularly troubling states. As seen from Fig. 7, there are states that have systematically smaller norm than the other states and some are even getting norm 1.0009 due to numerical issues.

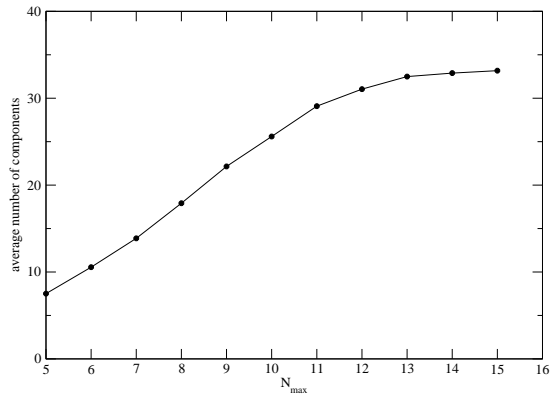


FIG. 6: Model space convergence of the Sturmian basis approach. The average number of components is the sum of the non-zero Sturmian basis components for the 47 occupied bound states divided by 47.

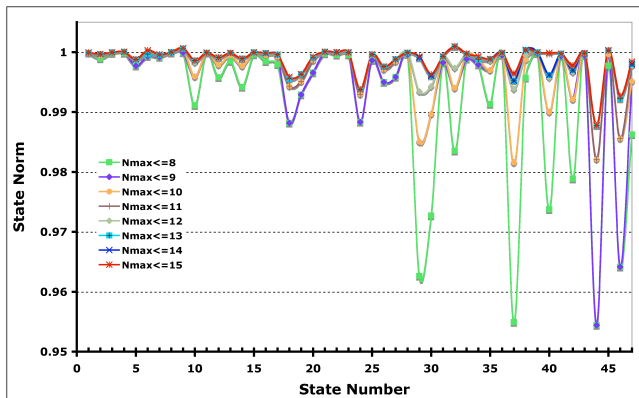


FIG. 7: Norm convergence as function of the model space.

It is possible that these troublesome features are actually result of a deeper numerical problem inherited in any standard large basis bound state technique. The problems are likely to be related to the fact that only the lowest states are well converged and thus possess the correct energy; because of that Sturmian states that are higher in n are less accurate, which is seen from the deviation of their actual energy from the desired Sturmian energy shown in Fig. 8. As seen from the top graph in Fig. 8 all basis states computed with WSBETA $N_{max} < 10$ have deviation within few keV. However, for larger model spaces $N_{max} > 9$ there are basis states whose deviation is getting much too big. This could become one of the main issues for the presented computational method.

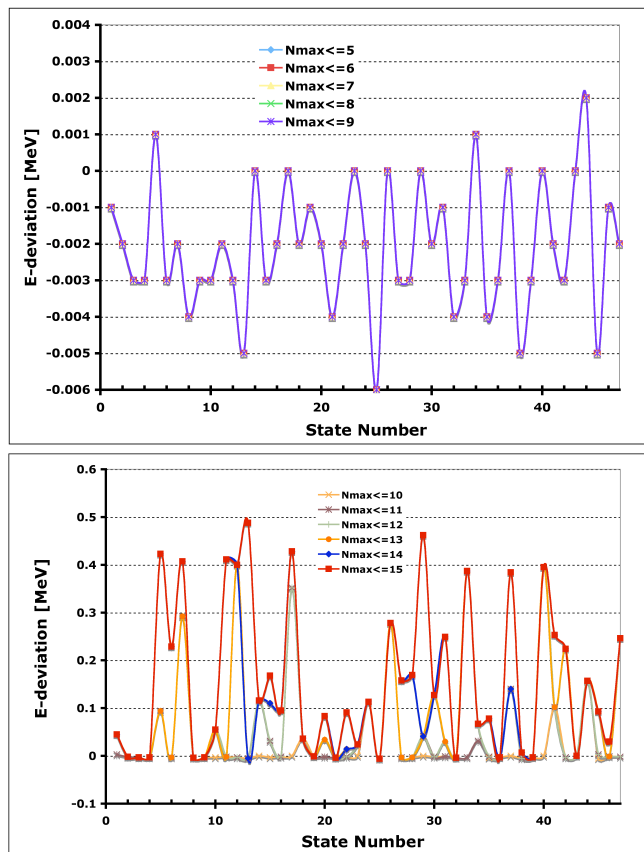


FIG. 8: Maximal deviation between the actually calculated eigenenergy of a basis state and the desired energy. Top graph: E-deviation for the model spaces $4 < N_{max} < 10$. Bottom graph: E-deviation for the spaces $9 < N_{max} < 16$.

D. Neutron pickup cross sections

The individual cross sections, for neutron transfer from a deformed state ψ_ν that results in a final state with J^π and energy E as shown in Fig. 5, are calculated as coherent cross sections with the code CHUCK3 [12] using the amplitudes c_{nlj}^ν times a Clebsch-Gordan coefficient and other appropriate factors [25]:

$$\sqrt{\frac{(1 + \delta_{0,K_i K_f})}{2j + 1}} D_0 \times c_{nlj}^\nu \times (J_f K_f | j m, J_i, K_i). \quad (15)$$

Here D_0 is the strength of the zero range transfer potential ($D_0 \delta(x)$, $D_0^2=18$ [11]). The resulting reaction cross sections defined for each single particle state $\sigma_\lambda(\epsilon_\nu, J^\pi)$ are shown in Fig. 9. In what follows the index λ will denote the equivalent pair of indexes (ϵ_ν, J^π) . The size of the circles reflects the size of the corresponding cross sections. As seen from Fig. 9 there is often a good overlap of the circles for the model spaces shown. This indicates the convergence of the calculated cross sections.

The cross sections that one can calculate within the presented framework correspond to sharp final states. In

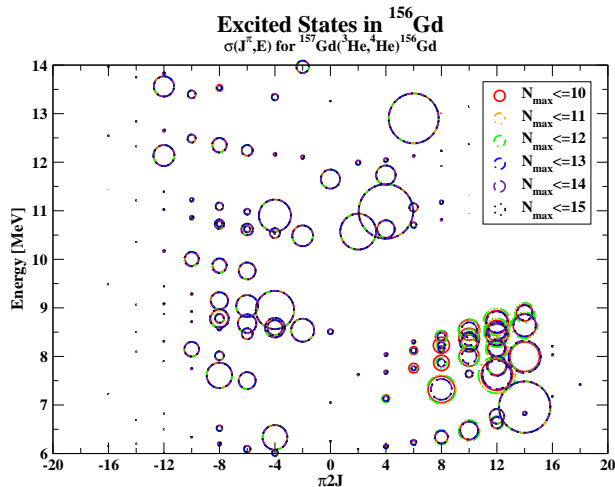


FIG. 9: Individual cross sections for neutron transfer from a deformed state that results in a final state with J^π and energy E as shown in Fig. 5. The size of the circles reflects the size of the corresponding cross sections.

reality there are widths associated with the single particle states as well as with the final states. In order to produce a smooth total cross section as a function of the excitation energy of the ^{156}Gd system we consider a Cauchy type smearing distribution function (Lorentzian) and define a smooth $\sigma(E)$ cross section [25]:

$$\rho_\lambda(E) = \frac{1}{2\pi} \frac{4\Gamma}{4(E - E_\nu)^2 + \Gamma^2} \quad (16)$$

$$\sigma(E) = \sum_\lambda \rho_\lambda(E) \sigma_\lambda, \quad \Gamma = a + bE.$$

In Fig.10 are shown the effects on the total cross section $\sigma(E)$ of different smearing width choices Γ . The choice of Γ should eventually be fixed by comparison of the theoretical and experimental cross sections.

For each choice of a model space N_{max} one can compute a set of cross sections $\sigma_\lambda(\epsilon_\nu, J^\pi)$. If the model space is sufficiently big so that convergence has been archived for the c_ν^{nlj} then one expects that the corresponding cross sections would be the same for the converged spaces. It was show in Fig. 6 that convergence requires $N_{max} > 12$. Therefore, as expected, the smeared total cross sections for $N_{max} > 12$ are the same as seen in Fig. 11.

E. The $P(J^\pi, E)$ distributions

The smeared cross sections, introduced in the previous section, can be used to define the probability to excite a state with quantum numbers J^π :

$$P(J^\pi; E) = \frac{1}{\sigma(E)} \sum_\lambda \delta_{J, J_\lambda} \delta_{\pi, \pi_\lambda} \rho_\lambda(E) \sigma_\lambda \quad (17)$$

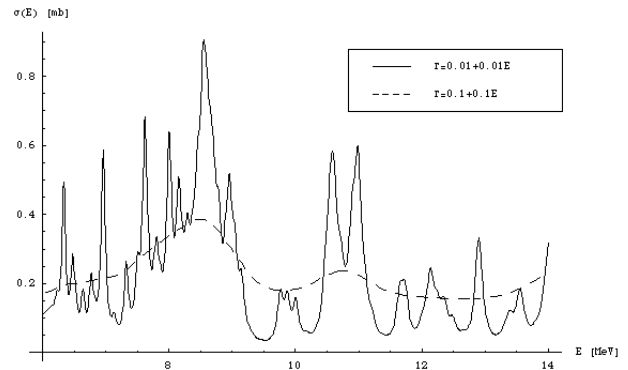


FIG. 10: Total neutron cross section $\sigma(E)$ in mb units smeared with Lorentzian using energy dependent width $\Gamma = a + bE$. Dashed line represents $\Gamma = 0.1 + 0.1E$ and continuous line represents $\Gamma = 0.01 + 0.01E$.

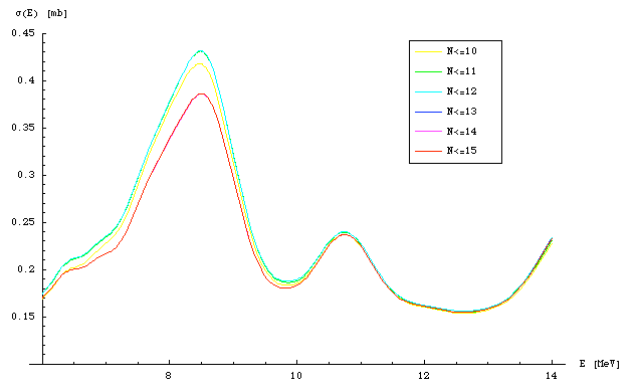


FIG. 11: Smeared total cross section for $\Gamma = 0.1 + 0.1E$ as a function of N_{max} . The identical $\sigma(E)$ for $N_{max} > 12$ (red curve) illustrate the convergence of the results.

It is clear that if one sums over all possible J^π quantum numbers then one gets one, that is, $\sum_{J^\pi} P(J^\pi; E) = 1$.

In Fig. 12 are shown the formal probabilities $P(J^\pi; E)$ for exciting J^π state of ^{156}Gd at energy E through direct neutron pickup via 42 MeV ^3He on ^{157}Gd target.

In Fig. 13 are shown $P(J^\pi; E)$ distributions that are of interest to the surrogate method. These graphs show that at least in principle there are no dead channels due to zero $P(J^\pi)$ and thus any channel that goes through $J < 8$ should be able to provide information on the decay probability of the compound system. The apparently zero values of the distribution for $J > 6$ are due to the model space used that focuses mostly on $J < 8$ excited states in ^{156}Gd .

IV. CONCLUDING REMARKS AND DISCUSSIONS

The present computational method is clearly a viable approach to particle pick-up reactions in deformed and

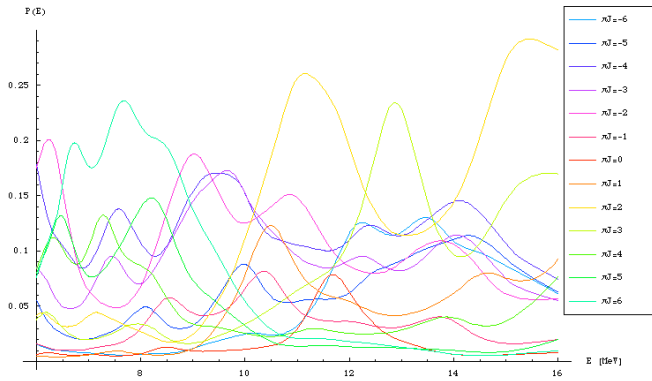


FIG. 12: All $P(J^\pi; E)$ distributions for $J < 8$.

strongly deformed systems. However, for stripping reactions the method would need to incorporate the effects of the pairing interaction since adding a nucleon would involve mostly levels near and above the Fermi level and even unbound states and resonances. In heavier nuclei the treatment of the valence single particle states above the Fermi level would probably face a problem due to the treatment of weakly bound states that may render the current computational technique useless; this could easily be monitored through evaluation of the norm of the bound states $\psi_{\varepsilon m}$ and the quality of the Sturmian basis $\phi_{\varepsilon n l j m}$. An alternative to the current approach that uses a standard bound state computational technique to compute the overlap of the state $\psi_{\varepsilon m}$ and $\phi_{\varepsilon n l j m}$ would be to extend Rost's code to include higher multipoles beyond the β_2 or to solve numerically for $\psi_{\varepsilon m}$ as generalized eigenvalue problem for non zero deformation using the Sturmian basis states $\phi_{\varepsilon n l j m}$.

The surrogate method (Fig. 1) assumes that the surrogate reaction populates J^π states of the intermediate nuclear system within the same energy range as the desired reaction. The method would certainly fail if the distribution $P(J^\pi, E)$ becomes zero for some relevant values of J^π at the relevant range of energies E since there would be no way of deducing the decay probabilities $g_\chi(J^\pi, E)$. If $P(J^\pi, E) = 0$ for a given J^π at an isolated energy E one could perhaps devise an analytic continuation for $g_\chi(J^\pi, E)$. Our calculations, however, show that within the assumptions and computational modeling the reaction ${}^3\text{He} + {}^{157}\text{Gd} \rightarrow {}^4\text{He} + {}^{156}\text{Gd}^*$ has a well behaved formation probability $P(J^\pi, E)$ (see Fig. 12 and Fig. 13) within a wide energy range relevant to the desired reaction ${}^{155}\text{Gd} + n \rightarrow {}^{156}\text{Gd}^*$. Therefore, given an experimental input on the decay probability $P_{\delta\chi}$ into an exit channel χ within the surrogate formation channel δ , one should in principle be able to determine $g_\chi(J^\pi, E)$.

Experimental input is essential for the fine tuning of the model parameters such as single particle Woods-Saxon potential, optical model potential for the incoming and out going projectiles as well as the choice of $\Gamma(E)$ used in the smearing function $\rho(E)$. Above all a compar-

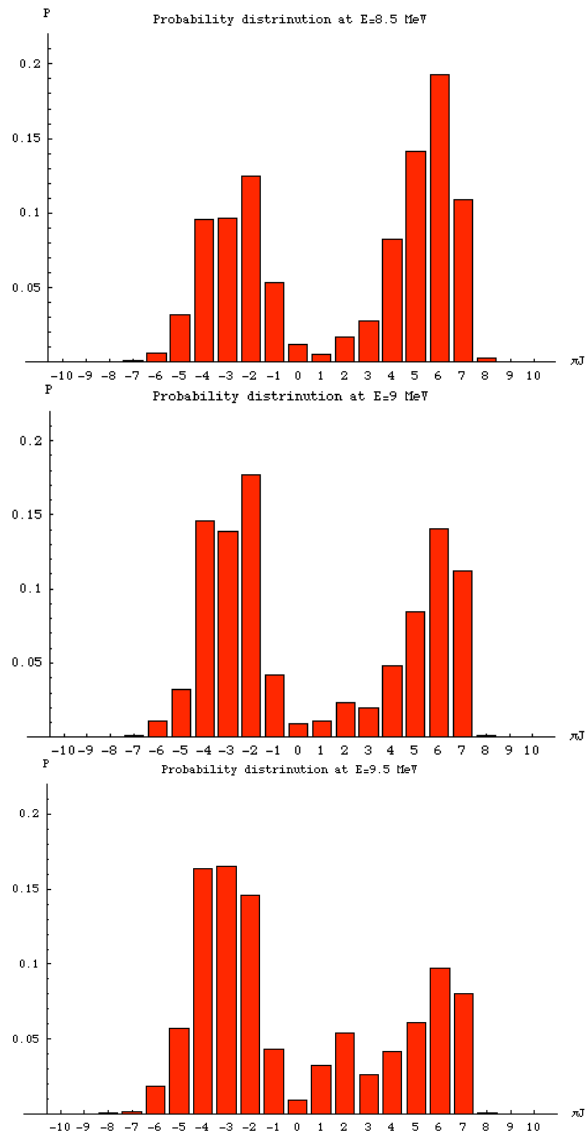


FIG. 13: $P(J^\pi; E)$ distributions for energies near the neutron separation energy in ${}^{156}\text{Gd}$. From top to bottom the energies are 8.5, 9, and 9.5 MeV. The sign of the horizontal coordinate corresponds to the parity π and its magnitude gives J .

ison with experiment should be the true measure of the applicability the surrogate method.

Acknowledgments

We would like to thank P. Navratil, J. P. Vary, and W. Younes for interesting and helpful discussions. This work was partly performed under the auspices of the U. S. Department of Energy by the University of California, Lawrence Livermore National Laboratory under contract No. W-7405-Eng-48. Support was also provided from the LDRD contract No. 04-ERD-057. Some of the calculations have been performed using the LLNLs Thunder machine.

V. APPENDIX

A. Ω_{\pm} splitting due to particle-core coupling

A more rigorous analysis in the intrinsic frame of the rotational energy of the hole in the core system gives:

$$\begin{aligned} & \langle \Omega_{\pm} | J \cdot T \cdot J | \Omega_{\pm} \rangle = \\ & = 2H_C - \frac{\hbar^2}{2\mathcal{I}_{\perp}} (\langle K | I^2 | K \rangle + \langle \nu | j^2 | \nu \rangle) \\ & - \frac{\hbar^2}{2\mathcal{I}_{\perp}} \left[\left(\frac{\mathcal{I}_{\perp}}{\mathcal{I}_{\parallel}} - 1 \right) (K^2 + \nu^2) \pm 2 \frac{\mathcal{I}_{\perp}}{\mathcal{I}_{\parallel}} K \nu \right] \end{aligned} \quad (18)$$

Here $\Omega_{\pm} = |K \pm \nu|$, J is the intrinsic angular momentum of the combined system (hole and core), I for the core, and j for the hole. H_C is the Coriolis coupling (11). T is the moment of inertia of the combined system. T is diagonal in the intrinsic frame with $T_x = T_y = 1/(2\mathcal{I}_{\perp})$ and $T_z = 1/(2\mathcal{I}_{\parallel})$.

For the shape and moment of inertia of rigid ellipsoid of mass M one has:

$$\begin{aligned} \mathcal{I}_i &= \frac{M}{5} \sum_j d_j^2 - d_i^2, \quad R(\theta, \phi) = R_0(1 + \beta Y_{20}(\theta, \phi)) \\ d_x = d_y &= 1 - \beta \frac{1}{4} \sqrt{\frac{5}{\pi}} \neq d_z = 1 + \beta \frac{1}{2} \sqrt{\frac{5}{\pi}} \end{aligned} \quad (19)$$

Which gives:

$$\frac{\mathcal{I}_{\perp}}{\mathcal{I}_{\parallel}} = \frac{32\pi + \beta(25\beta + 8\sqrt{5\pi})}{2(\sqrt{5}\beta - 4\sqrt{\pi})^2} \quad (20)$$

B. c_{ν}^{nlj} amplitudes in a Sturmian basis

As we already mentioned, for strong deformation one needs to consider either the full Taylor expansion [6] or to use numerical methods to solve the Schrödinger equation [7]. Given the code WSBETA [7] along with the code DWUCK [29] plus a few post-processing codes one can solve the Sturmian problem and find expansion of any deformed state $\psi_{\varepsilon m}$ ($\beta \neq 0$) in terms of non-orthogonal Sturmian states $\phi_{\varepsilon nljm}$ with correct tails given by their binding energy ε .

$$\psi_{\varepsilon m} = \sum_{nlj} c^{nlj} \phi_{\varepsilon nljm} \quad (21)$$

For this purpose, one solves the following set of eigenvalue equations:

$$\begin{aligned} H_{\beta \neq 0} \psi_{\varepsilon \Omega} &= \varepsilon \psi_{\varepsilon \Omega} \\ H_{\beta=0} \phi_{\varepsilon nljm} &= \varepsilon \phi_{\varepsilon nljm} \end{aligned} \quad (22)$$

Since WSBETA gives solutions to these problems in the same cylindrical harmonic oscillator basis $|NN_z\Lambda\rangle$, one

can evaluate the overlap matrix of these states:

$$\begin{aligned} \phi_{\varepsilon nljm} &= \sum_{NN_z\Lambda} D_{nljm}^{NN_z\Lambda} |NN_z\Lambda m\rangle \\ \psi_{\varepsilon \Omega} &= \sum_{NN_z\Lambda} B_{\Omega}^{NN_z\Lambda} |NN_z\Lambda \Omega\rangle \end{aligned}$$

Here the quantum numbers N, N_z, Λ , and m represent the total number of oscillator quanta, the number of oscillator quanta in the z -direction, and the projection of the angular momentum and the total angular momentum onto the symmetry axis z . Since Sturmian states $\phi_{\varepsilon nljm}$ with different ljm quantum numbers are orthonormal due to orthogonality of the spin and angular momentum components, we have non-orthogonality only within a fixed ljm sub-set:

$$\mu_{nk}^{ljm} = \langle \phi_{\varepsilon nljm} | \phi_{\varepsilon kljm} \rangle = \sum_{NN_z\Lambda} \bar{D}_{nljm}^{NN_z\Lambda} D_{kljm}^{NN_z\Lambda} \quad (23)$$

$$\Xi_{nljm} = \langle \phi_{\varepsilon nljm} | \psi_{\varepsilon m} \rangle = \sum_{NN_z\Lambda} \bar{D}_{nljm}^{NN_z\Lambda} B_m^{NN_z\Lambda} \quad (24)$$

In order to determine the coefficients c^{nlj} in (21) we have to use the inverse μ_{ljm}^{nk} of the overlap μ_{nk}^{ljm} ($\sum_k \mu_{nk} \mu^{n'k} = \delta_n^{n'}$). Within each sub-space of fixed lj we have:

$$\Xi_n = \sum_k c^k \mu_{nk} - \text{fixed } lj \Rightarrow c^n = \sum_k \mu^{nk} \Xi_k$$

In general one expects to have no problems in inverting μ_{nk} since $\det \mu = 0$ would imply linear dependence of the vectors $\phi_{\varepsilon nljm}$ which should not be present since each of these states has different number of nodes. How many Sturmian states $\phi_{\varepsilon nlj}$ are needed is determined by the normalization condition:

$$\|\psi_{\varepsilon \Omega}\|^2 = 1 \geq \sum_{lj} \sum_{nk} \bar{c}^n \mu_{nk} c^k = \sum_{lj} \sum_n \bar{c}^n \Xi_n$$

Therefore the number N_S of Sturmian states $\phi_{\varepsilon nlj}$ is determined by the normalization requirement:

$$\sum_{lj}^{j_{\max}} \sum_{n,k}^{N_S} \bar{\Xi}_n \mu^{nk} \Xi_k = 1 \quad (25)$$

Here an implicit lj index is assumed for Ξ_n and μ^{nk} . Since parity considerations determine the value of l for any given j one can write all lj indexed partitions as single j index.

When the asymptotic tail is proper (22) and N_S and j_{\max} are such that the normalization condition (25) is satisfied then one can be sure that there are no states omitted, continuum or discrete, because we have normalized bound state with the correct expansion at small r as well as at large r .

C. Phase conventions for the wave functions

The overall phase of a wave function, single particle wave function in particular, is arbitrary and unobservable. Thus, it is usually fixed for convenience by a suitable choice of convention. Although there could be as many conventions as wave function, there are two main choices in the literature. One convention is to consider wave functions that are positive as $r \rightarrow \infty$ [11, 12]. Another convention is to consider wave functions that are positive at the origin $r \rightarrow 0$ [5]. Sometime the convention

is not clear at all [7].

For our calculations, it is important to adjust the c'_{nlj} since we use two different codes [7, 12]. First the c'_{nlj} are calculated from the WSBETA [7] wave functions as described in Appendix section V B. Then we take into account the phase difference relative to the wave functions generated by DWUCK4 and CHUCK3 [11, 12]. For this purpose, we evaluate the sign of the WSBETA spherical wave functions that are given in cylindrical basis at $\theta = \pi/3$, $\phi = 0$, and $r \rightarrow \infty$ using an asymptotic expression of the cylindrical basis wave functions.

-
- [1] C. W. Reich, Nuclear Data Sheets **99**, 753 (2003).
 [2] A. Bohr and B. R. Mottelson, *Nuclear Structure I: Single-Particle Motion*, vol. 1 (W. A. Benjamin, Inc., 1969).
 [3] A. Bohr and B. R. Mottelson, *Nuclear Structure II: Nuclear Deformation*, vol. 2 (W. A. Benjamin, Inc., 1975).
 [4] R. D. Woods and D. S. Saxon, Phys. Rev. **95**, 577 (1954).
 [5] B. Hird and K. H. Huang, Comp. Phys. Comm. **10**, 293 (1975).
 [6] N. K. Glendenning, *Direct Nuclear Reactions* (World Scientific, 2004).
 [7] S. Cwiok, J. Dudek, W. Nazarewicz, J. Skalski and T. Werner, Comp. Phys. Comm. **46**, 379 (1987).
 [8] B. Hird, Comp. Phys. Comm. **6**, 30 (1973).
 [9] B. Mohammed-Azizi and D. E. Medjadi, Comp. Phys. Comm. **156**, 241 (2004).
 [10] E. Rost, Phys. Rev. **154**, 994 (1967).
 [11] P. D. Kunz, *Computer code dwuck4* (1990), URL <http://spot.colorado.edu/~kunz/>.
 [12] P. D. Kunz, *Computer code chuck3* (1992), URL <http://spot.colorado.edu/~kunz/>.
 [13] B. Hird and K. H. Huang, Can. J. Phy. **53**, 559 (1975).
 [14] R. G. Helmer, Nuclear Data Sheets **103**, 565 (2004).
 [15] G. R. Satchler, Ann. Phys. **3**, 275 (1958).
 [16] N. Azziz and A. Covello, Nucl. Phys. A **123**, 681 (1969).
 [17] R. W. Richardson, Phys. Rev. **144**, 874 (1966).
 [18] J. Dukelsky, V. G. Gueorguiev, P. V. Isacker, S. Dimitrova, B. Errea, and S. Lerma H., Phys. Rev. Lett. **96**, 072503 (2006).
 [19] F. Pan, V. G. Gueorguiev, and J. P. Draayer, Phys. Rev. Lett. **92**, 112503 (2004).
 [20] T. Papenbrock and A. Bhattacharyya, Phys. Rev. C **75**, 014304 (2007).
 [21] I. Kanestrøm and P. O. Tjøm, Nucl. Phys. A **138**, 177 (1969).
 [22] P. C. Joshi and P. C. Sood, Phys. Rev. C **9**, 1965 (1974).
 [23] J. C. Peng, J. V. Maher, G. H. Wedberg, and C. M. Cheng, Phys. Rev. C **13**, 1451 (1976).
 [24] C. Granja, S. Pospisil, A. Aprahamian, H. Borner, H. Lehmann, T. von Egidy, H.-F. Wirth, G. Graw, R. Hertenberger, Y. Eisermann, et al., Phys. Rev. C **70**, 034316 (2004).
 [25] B. L. Andersen, B. B. Back, and J. M. Bang, Nucl. Phys. A **147**, 33 (1970).
 [26] T. Belgya, O. Bersillon, R. Capote, T. Fukahori, G. Zhigang, S. Goriely, M. Herman, A.V. Ignatyuk, S. Kailas, A. Koning, P. Oblozinsky, V. Plujko and P. Young., *Handbook for calculations of nuclear reaction data, RIPL-2* (IAEA, Vienna, 2006), URL <http://www-nds.iaea.org/RIPL-2/>.
 [27] F. D. Becchetti and G. W. Greenlees, Phys. Rev. **182**, 1190 (1969).
 [28] V. Avrigeanu, P.E.Hodgson, and M. Avrigeanu, Phys. Rev. C **49**, 2136 (1994).
 [29] DWUCK or any other code that can provide search on the potential depth for a fixed binding energy is needed to determine the potential strength needed to place the nlj spherical state at the desired binding energy.